Editors' Suggestion

Contact line friction of electrowetting actuated viscous droplets

Quoc Vo and Tuan Tran*

School of Mechanical and Aerospace Engineering, Nanyang Technological University, 50 Nanyang Avenue, 639798, Singapore

(Received 1 March 2018; published 1 June 2018)

We examine the contact line friction coefficient of viscous droplets spreading and retracting on solid surfaces immersed in ambient oil. By using the electrowetting effect, we generate a surface tension imbalance to drive the spreading and the retracting motion of the three-phase contact line (TCL). We show that neither the driving force intensity nor TCL direction significantly influences the friction coefficient. Instead, the friction coefficient depends equivalently on the viscosity of liquid droplets and the surrounding oil. We derive and experimentally verify a transient timescale that can be used to characterize both the spreading and retracting dynamics.

DOI: 10.1103/PhysRevE.97.063101

I. INTRODUCTION

When a liquid droplet comes into contact with a solid substrate, its spreading motion is driven by an imbalance in interfacial tensions at the three phase contact line and opposed by both friction at the contact line and liquid inertia. Contact line motion is found not only in natural spreading or retracting of liquid [1], but also in other capillary-related phenomena such as evaporation, Marangoni-driven flows, and electrowetting [2–5]. Contact line motion also plays a central role in numerous technological and industrial applications ranging from digital microfluidics [6], dip coating, oil extraction to pesticides deposition [2]. A physical understanding of contact line dynamics is therefore of both fundamental and practical interests.

The contact line dynamics of a droplet spreading on a solid substrate are typically categorized into two main regimes. In the so-called underdamped regime, liquid inertia dominantly resists the contact line motion, resulting in apparent oscillations at the droplet's surface [7–9], whereas in the so-called overdamped regime, the viscous effect becomes dominant causing the droplet to spread or retract gradually to its equilibrium state [7,10–12]. In particular, contact line friction mostly dissipates excessive interfacial energy in the overdamped regime [13–15].

The contact line friction was shown to depend on both the viscosity μ of the fluid in the droplet [9,14] and the viscosity $\mu_\circ$ of the surrounding fluid [16]. The functional dependence of the contact line friction coefficient λ on μ and $\mu_\circ$ has been the subject of extensive, split research efforts. When $\mu_\circ$ is kept fixed, λ is typically represented in the form $\lambda \sim \mu^\alpha$, where α is a constant sensitive to the spreading velocity. On one hand, it was found experimentally that $\alpha = 1/2$ at the early stage, i.e., high spreading velocity, of capillary-driven spreading of droplets on solid surfaces in air [14,17,18]; a similar value of α was found for electrowetting-driven spreading of droplets in air [9]. On the other hand, $\alpha = 1$ was reported from theoretical [11] and experimental investigations for droplets spreading at the later stage, i.e., low spreading velocity, of glycerol solution droplets on glass substrates [19].

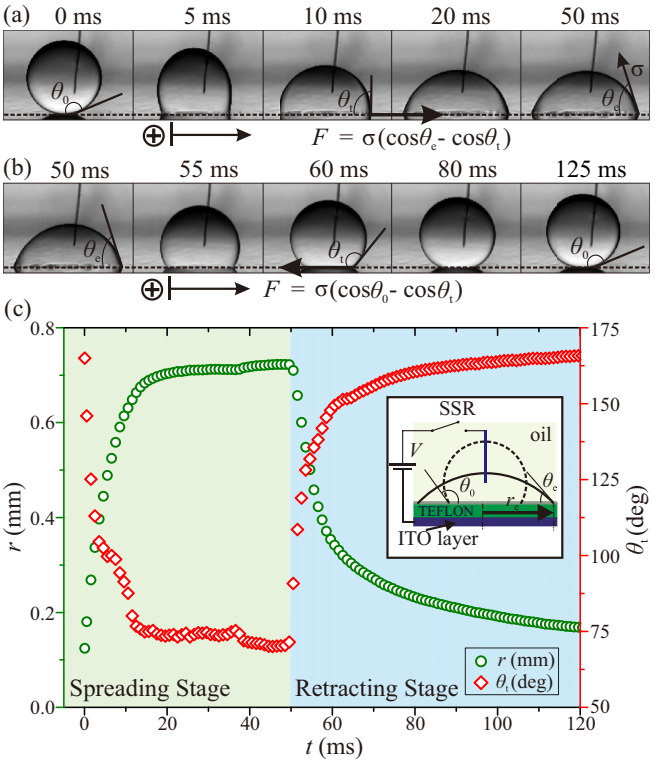

FIG. 1. (a) When a potential difference between a droplet and a substrate is applied, the droplet spreads from an initial state with contact angle θ_0 to a new equilibrium state with contact angle θ_e. At any transient state with contact angle θ_t, the driving force per unit length at the contact line is calculated as $F = \sigma(\cos\theta_e - \cos\theta_t)$. The positive direction of the contact line motion is indicated by the + sign. (b) When the voltage is released, the droplet retracts freely and the contact angle changes from θ_e to θ_0, assuming sufficiently small hysteresis. The driving force is now $F = \sigma(\cos\theta_0 - \cos\theta_t)$. (c) Typical plots of the contact radius r versus time t (left axis) and contact angle θ_t versus time t (right axis) for a droplet of initial radius $R = 0.5$ mm when a voltage $V = 100$ V is applied for 50 ms and then released. Inset: schematic of the experimental setup. The liquid used to generate droplets is water-glycerol solution having viscosity $\mu = 17.6$ mPas. The outer phase is silicone oil having viscosity $\mu_o = 4.6$ mPas.

*Corresponding author: ttran@ntu.edu.sg

The dependence of λ on $\mu_\circ$ has also been the subject of numerous theoretical and experimental studies. Miller *et al.* [20] showed equal contributions of both viscosities μ and $\mu_\circ$ to the decaying factor of droplet oscillations. Huh *et al.* [21] used a creeping flow model to describe the contact line velocity and found that the ratio of the two viscosities had an important role on the contact line motion. More recently, Hong *et al.* [16] reported a power law relation $\lambda \sim \mu_\circ^{0.8}$ from an experimental study of electrowetting actuated droplets on Teflon surfaces in silicone oils.

Nonetheless, numerous standing questions remain open, in particular how the transient dynamics of contact line depends on contributing factors such as contact line friction, liquid viscosity, and inertia. A systematic investigation of the transient dynamics therefore is needed to broaden the current understanding of contact line motion and its role in related phenomena.

In this paper, we consider the contact line motion of aqueous droplets on a solid surface. We focus on the case in which the contact line motion is solely caused by interfacial tension imbalance, while excluding the Marangoni and evaporation effects by immersing the tested droplet and surface in an oil pool. We use the electrowetting effect to induce the contact line motion of droplets. By applying a potential difference between a droplet and the surface we generate an interfacial tension imbalance at the contact line, causing the droplet to spread to a new equilibrium state [Fig. 1(a)]. Once the droplet is in the new equilibrium state, removing the potential difference restores the surface energy to the original state, thus imposing a surface tension imbalance in the opposite direction and drives the droplet to retract [Fig. 1(b)]. We then investigate the contact line friction and its role in the transient dynamics in both the spreading and retracting stages. By considering this system in a parameter space of viscosities μ, $\mu_\circ$, and driving force intensity set by the applied voltage, we aim to achieve a unified description of the dependence of λ on both μ and $\mu_\circ$ at the high viscosity limit.

II. MATERIALS AND METHODS

In our experiments, we use aqueous glycerin solutions consisting of glycerol, DI water, and 0.125 M sodium chloride as the working fluids to generate droplets. By adjusting the glycerol concentration ζ, we vary the viscosity μ of the solutions from 8.2 mPas to 615.0 mPas. The exact concentrations and corresponding physical properties are given in Table I. We use silicone oils with viscosity in the range $1.8\,\text{mPas} \leqslant \mu_\circ \leqslant 970.0\,\text{mPas}$ as the surrounding fluids. The temperature of the oil pool is kept at $20 \pm 0.5\,^\circ\text{C}$ to maintain consistent experimental conditions. We note that varying ζ has a minute effect on the interfacial tension σ between the working fluids and the surrounding oils [16]; we experimentally measured σ and verified that it varied in a narrow range, from 30.8 mNm^{-1} to 24.9 mNm^{-1}, for ζ varying from 55 % to 95 % (Table I).

In the inset of Fig. 1(c), we show a schematic of our experimental setup. A droplet is seated on an indium tin oxide (ITO) glass slide covered by a fluoropolymer layer (Teflon AF-1600, DuPont) of thickness $d = 2.5\,\mu\text{m}$. The Teflon layer acts as a hydrophobic and electrically insulating cover. By immersing both the droplets and the substrate in silicone oil,

TABLE I. Measured values of viscosity μ of glycerin solutions and interfacial tensions σ between glycerin solutions and silicone oils. Here, ζ is the mass concentration of glycerol in the solutions; $\sigma_{(2\,\text{cSt})}$ and $\sigma_{(5\,\text{cSt})}$, respectively, denote the interfacial tensions of the solutions in 2 cSt and 5 cSt silicone oils.

ζ (%wt)	μ (mPas)	$\sigma_{(2\,\text{cSt})}$ (mN m^{-1})	$\sigma_{(5\,\text{cSt})}$ (mN m^{-1})
55	8.2	29.7	30.8
67	17.6	26.9	26.9
74	32.7	25.9	27.4
80	68.7	26.8	26.3
86	136.0	24.9	25.6
91	258.8	26.0	25.2
95	615.0	27.5	28.2

the static contact angles of droplets are close to 180°. To induce the electrowetting effect on a droplet, we immerse one end of a 18 μm diameter tungsten wire into the droplet and connect the other end of the wire to the positive terminal of a DC power supply. The negative terminal of the power supply is connected to the ITO layer which acts as the ground electrode. We generate an electrical pulse in the form of a step function between the wire and the ITO layer by using a solid state relay (SSR). The amplitude V of the applied voltage is varied in the

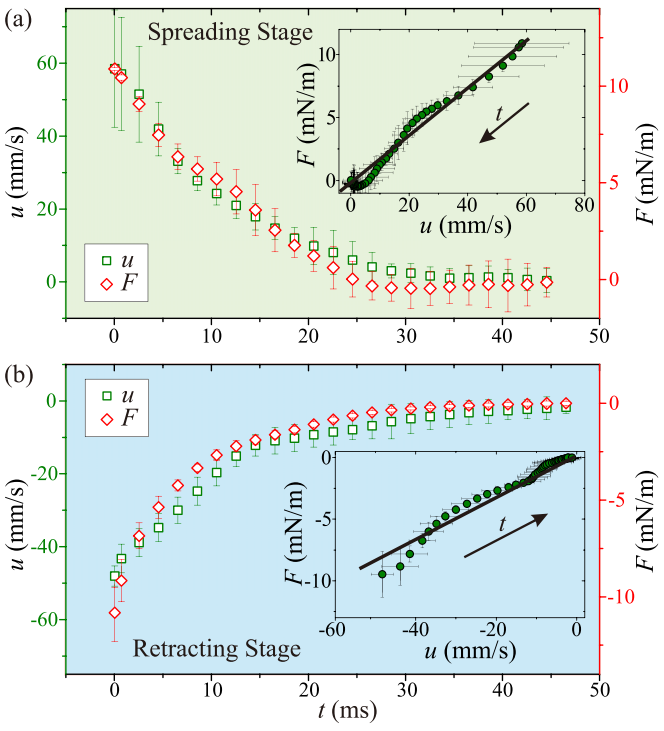

FIG. 2. Plots of contact line velocity u versus time t (left axis) and contact line force, F versus time t (right axis) for the spreading stage (a) and the retracting stage (b). Insets: data in the main plots are replotted to show the relation between F and u. The results were obtained by applying 80 V to a 1 mm diameter droplets ($\mu = 8.2$ mPas) immersed in silicone oil ($\mu_\circ = 4.6$ mPas). The best fits to the data in the insets give $\lambda = 0.19 \pm 0.01$ Pas for the spreading stage and $\lambda = 0.17 \pm 0.02$ Pas for the retracting stage.

range $20\,\mathrm{V} \leqslant V \leqslant 100\,\mathrm{V}$. We note that all of our experiments are carried out without contact angle saturation[4], which occurs at $V = 115\,\mathrm{V}$ with our experimental configurations [7]. To make sure that the droplet reaches its new equilibrium, the applied voltage is maintain for a sufficient period, i.e., 50 ms [see Fig. 1(c)]. Subsequently, we release the voltage for the droplet to retract freely and observe the retracting stage. We observe that the droplet reacts almost immediately after the circuit is closed or opened, suggesting that the time duration for the system to electrically charge or discharge is negligible compared to its hydrodynamical response time [22,23]. We use a high-speed camera (SAX2, Photron) to record both the spreading and retracting motions. The recording is taken from side view (see snapshots in Figs. 1(a) and 1(b) with a typical frame rate 5000 frames per second and a spatial resolution of 4 microns per pixel.

We repeat the experiment three times for each set of the control parameters, (V,μ,μ_o), and extract both the base radius r and the contact angle θ_t as functions of time t. Here, θ_t is the so-called Lippmann contact angle [24], which is measured at some distance away from the contact line vicinity. Repetitive measurements of r and θ_t typically result in less than 5% deviation. We observe insignificant hysteresis of the system evidenced by the negligible difference between the initial state before spreading and the final state after retracting [e.g., see first of Fig. 1(a), and last snapshots of Fig. 1(b)]. This may result from entrapment of a thin oil layer between the droplet and the substrate during the spreading stage [16,23,25,26]. We also observe that r and θ_t vary monotonically with time in both the spreading and the retracting stages due to the high viscosity of working fluids [Fig. 1(c)]. In other words, the contact line dynamics in both of these stages are overdamped.

In the absence of hysteresis, one can write the expression for the driving force per unit length F at the contact line based on the interfacial tension imbalance in the horizontal direction:

$$F = \begin{cases} \sigma(\cos\theta_e - \cos\theta_t), & \text{(spreading stage)} \\ \sigma(\cos\theta_0 - \cos\theta_t), & \text{(retracting stage)} \end{cases}, \qquad (1)$$

where θ_0 and θ_e, respectively, are the initial contact angle and the equilibrium contact angle after spreading, and θ_t is the contact angle at time t. Here, the spreading direction is assigned positive Figs. 1(a) and 1(b). Both values of F and contact line velocity $u = dr/dt$ can be calculated using the measured values of θ_t and r at time t. In Fig. 2, we show the dependence of F and u on t in both the spreading stage [Fig. 2(a)] and the retracting stage [Fig. 2(b)]. The similarity between two functions $F(t)$ and $u(t)$ suggests a linear relation:

$$F = \lambda u. \qquad (2)$$

Here, λ is the so-called friction coefficient representing the three-phase contact line (TCL) friction, which originates from interactions between the liquid molecules and the solid surface at TCL [11]. We note that the linear relation between F and u is applicable for small TCL velocity [11] and is consistent with the data shown in the insets of Figs. 2(a) and 2(b).

III. RESULTS AND DISCUSSIONS

A. Effects of motion direction and driving force on contact line friction coefficient

For a fixed set of the parameters $(V,\mu,\mu_\circ)$, we obtain the friction coefficients in both the spreading and retracting stages. The difference between these coefficients is typically within 15% of their mean value, suggesting that the friction coefficient is independent of the TCL direction. This result is consistent with the negligible hysteresis observed before and after applying the electrowetting effect.

We now examine the effect of driving force on the friction coefficient. The magnitude of F, which is varied by changing the applied voltage, may be characterized by the maximum force per unit length acting on the TCL

$$F_{max} = \sigma(\cos\theta_e - \cos\theta_0) = \eta\sigma, \qquad (3)$$

where $\eta = \cos\theta_e - \cos\theta_0$ represents the change in wettability of the solid surface when the contact angle changes from the initial value θ_0 to the new equilibrium one θ_e. In electrowetting context, η is termed electrowetting number and is related to electrical properties of the system by the Young-Lippmann equation

$$\eta = \cos\theta_e - \cos\theta_0 = \frac{\epsilon\epsilon_0 V^2}{2d\sigma}, \qquad (4)$$

where V is the applied voltage, d is the insulating layer thickness, and ϵ, ϵ_0 are the permittivities of the insulating layer and free space, respectively. It follows that η also represents the electrical strength compared to the interfacial tension between the glycerin solution and the surrounding oil [4]. As a result, by varying the voltage V, we change the characteristic force F_{max} acting on the contact line.

In Fig. 3, we plot the dependence of F on u for various applied voltages. In this particular experiment, we generate

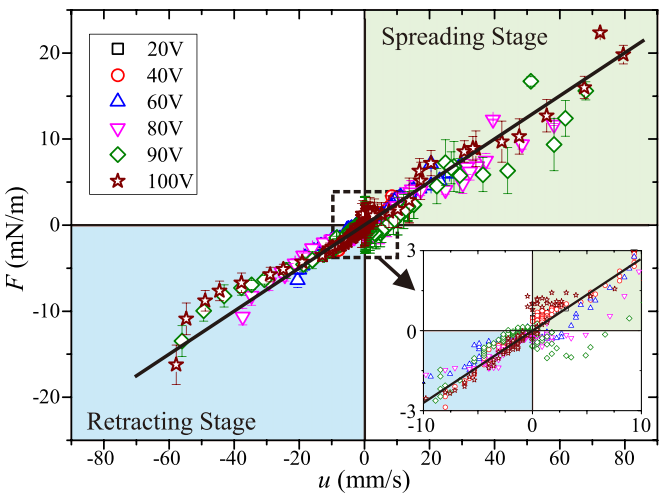

FIG. 3. Driving force F at the contact line versus contact line velocity u for different applied voltages ($20\,\mathrm{V} \leqslant \mathrm{V} \leqslant 100\,\mathrm{V}$). Inset: zoom in of data near the origin. The working fluid's viscosity is $\mu = 17.6\,\mathrm{mPas}$, while the oil viscosity is $\mu_o = 4.6\,\mathrm{mPas}$. The radius of droplets is 0.5 mm. The friction coefficient $\lambda = 0.28 \pm 0.05\,\mathrm{Pas}$ is calculated from the slope of the solid line.

droplets from a mixture of glycerol solution and sodium chloride with viscosity $\mu = 17.6$ mPas. The surrounding oil has viscosity $\mu_o = 4.6$ mPas (see Table I for material properties). The varying range of V is $20\,\text{V} \leqslant V \leqslant 100\,\text{V}$, resulting in $0.05 \leqslant \eta \leqslant 1.27$ and subsequently $1.37\,\text{mNm}^{-1} \leqslant F_{\max} \leqslant 34.2\,\text{mNm}^{-1}$. The overlapping of different datasets obtained using various values of V regardless of the TCL direction indicates that both the characteristic driving force $F_{\max}$ and TCL direction, i.e., spreading or retracting, have no significant effect on the contact line friction coefficient λ. This is also consistent with the reported results of water droplets spreading in air using electrowetting [27].

B. Effects of viscosity on contact line friction coefficient

To study the effect of viscosities of the two involving phases on λ, we fix the applied voltage at 80 V and vary both μ and $\mu_\circ$ to observe the resulting change in λ. In Fig. 4(a), we show a log-log plot of the measured values of λ versus μ while keeping μ_o fixed at 4.6 mPas. The viscosity μ is varied from 8.2 mPas to 615.0 mPas. The data obtained in both spreading and retracting stages are consistent with the scaling law $\lambda \sim \mu^{1/2}$. We note that the $1/2-$ scaling is also consistent with several previously reported datasets, e.g., for spreading of glycerol droplets on surfaces coated by Teflon [9,14], silicon dioxide (SiO_2) [14], and silane [14]. The vertical shifts between datasets reflect variations in surface properties, e.g., roughness, surface chemistry, and the surrounding phase, e.g., air or silicone oil. Similarly, we show in Fig. 4(b) the dependence of λ on $\mu_\circ$ in log-log scale for $1.8\,\text{mPas} \leqslant \mu_\circ \leqslant 970.0$ mPas, while keeping μ fixed at 17.6 mPas. Our data are also consistent with the scaling law $\lambda \sim \mu_o^{1/2}$ and agree well with the data collected for aqueous sodium chloride droplets on surfaces coated by Teflon and surrounded by silicone oils [16]. Our data therefore reveal that the dependence of λ on either μ or $\mu_\circ$ follow scaling laws with the same exponents, suggesting that μ and μ_o contribute *equally* to variations in λ. In other words, the dependence of λ on μ and μ_o reduces to

$$\lambda = C(\mu\mu_o)^{1/2} \tag{5}$$

for the tested ranges of μ and μ_o. Here, C is a constant that depends on surface properties [14]. In Fig. 4(c), we show a log-log plot of λ versus $\mu\mu_o$ for our datasets, which collapse to a single curve, confirming that Eq. (5) can be used to unify the dependence of λ on both μ and μ_o. A best fit to the our data gives $C = 26.24 \pm 4.6$, a constant specific to the properties of our substrate [Fig. 4(c), inset]. Although Eq. (5) works for the spreading and retracting dynamics of aqueous droplets in oils, it should be used with caution when the inner and outer phases have highly contrasted properties, e.g., aqueous droplets in air [21]. An extrapolation of this scaling law to such situation may require significant investigations towards the lower limit of $\mu_\circ$, thus merit a separate study.

C. The role of contact line friction on transient dynamics

We now examine effects of contact line friction on transient dynamics of the spreading and retracting stages. We note that beside contact line friction, viscous dissipation caused by large velocity gradient in liquid bulk may contribute significantly to

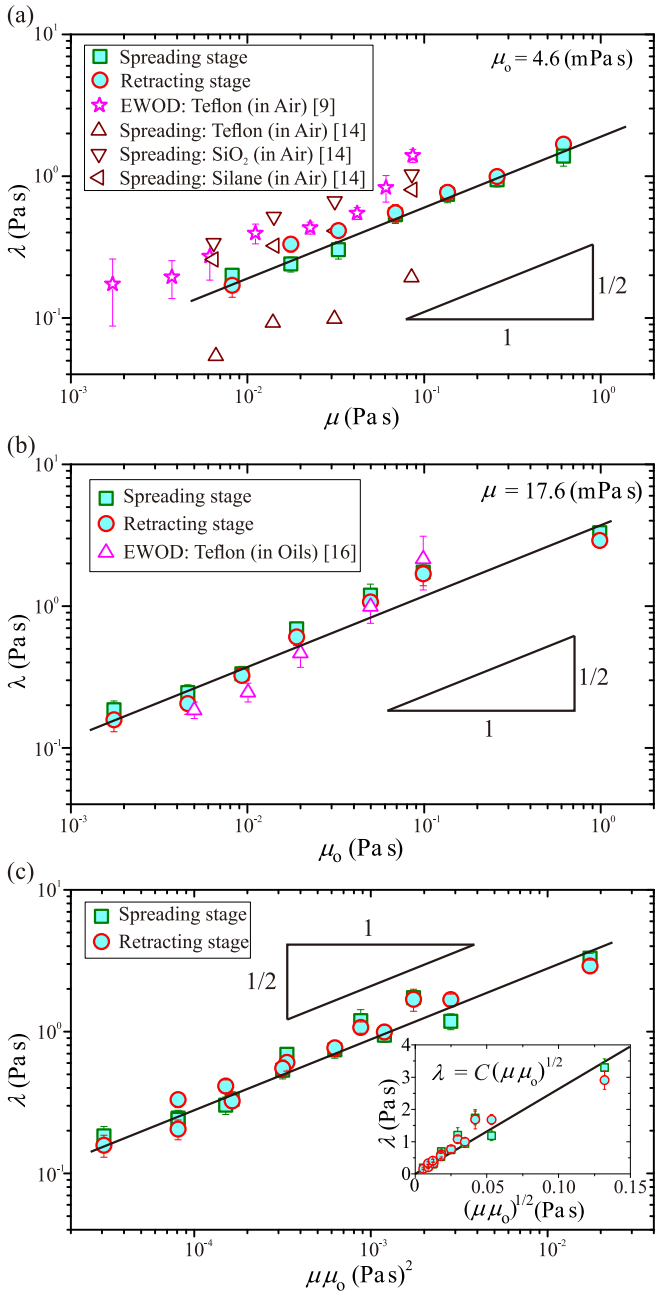

FIG. 4. (a) Log-log plot of λ versus viscosity μ when μ_o is fixed at 4.6 mPas. The solid line represents the scaling law $\lambda \sim \mu^{1/2}$. (b) Log-log plot of λ versus μ_o when μ is fixed at 17.6 mPas. The solid line represents the scaling law $\lambda \sim \mu_o^{1/2}$. (c) Log-log plot of λ versus $\mu\mu_o$ for our experimental data shown in (a) and (b). The solid line represents the scaling law $\lambda \sim (\mu\mu_o)^{1/2}$. Inset: Linear plot of λ versus $(\mu\mu_o)^{1/2}$. The solid line represents the relation $\lambda = C(\mu\mu_o)^{1/2}$, where $C = 26.24 \pm 4.6$ is the fitting parameter.

the transient dynamics, e.g., in the case of droplet oscillations [28] or imbibition of liquid in microchannels by electrowetting [29]. In our present analysis, the viscous dissipation in the bulk is assumed negligible as the system is in the overdamped regime with small velocity gradient. This assumption enables us to determine the characteristic timescale of the transient dynamics. On one hand, the characteristic velocity of the three

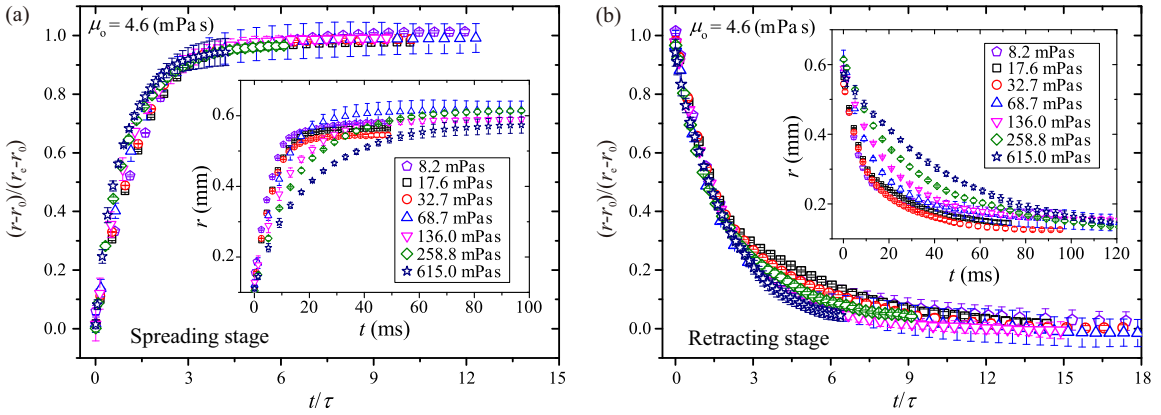

FIG. 5. Linear plots of the collapsed data of experiments with different droplet's viscosity μ for spreading stage (a) and retracting stage (b). The raw data of each plot is shown by the corresponding inset.

phase contact line (TCL) can be defined as $U = F_{\max}/\lambda$, or by incorporating Eqs. (3) and (5): $U = \eta\sigma/C(\mu\mu_o)^{1/2}$. On the other hand, if we denote τ the characteristic timescale for a droplet to switch between two equilibrium states, τ can be calculated as $\tau = (r_e - r_0)/U$, or

$$\tau = \frac{C(\mu\mu_o)^{1/2}(r_e - r_0)}{\eta\sigma}. \tag{6}$$

In Figs. 5 and 6, we respectively show the plots of $(r - r_0)/(r_e - r_0)$ versus t/τ for different values of μ and μ_o. The data collapse in both spreading and retracting stages, confirming that τ is indeed the characteristic timescale for the transient dynamics of viscous droplets actuated in ambient oils. We note that the dependence of τ on the electrical parameter η has two interesting implications: the transient dynamics of a droplet depends on 1) the strength of the electrical driving force when the droplet spreads due to the electrowetting effect because $\eta = \epsilon\epsilon_0 V^2/2d\sigma$, and 2) the initial condition when the droplet retracts from an equilibrium state where the contact angle is θ_e because $\eta = \cos\theta_e - \cos\theta_0$. This observation may be helpful in considering the spreading and retracting dynamics of droplets in other phenomena such as droplet impact [30], or wetting and dewetting of liquid films and droplets [2,31].

IV. CONCLUSIONS

In summary, we investigate the friction coefficient λ of viscous droplets in both the spreading and retracting stages: the spreading motion is driven by the electrowetting effect, whereas the retracting motion is purely driven by capillarity. We show that while λ depends weakly on either the driving force's strength or the moving direction of the contact line, it depends equally on both the viscosity μ of the droplets and the viscosity μ_o of the surrounding oils. Based on the dependence of λ on μ and $\mu_\circ$, we derive and experimentally verify a unifying characteristic timescale for both the spreading and retracting stages. The proposed timescale is valid in both spreading and retracting stages suggesting that it may be applied in other interfacial tension driven problems such as droplet wetting or impacting on solid surfaces.

ACKNOWLEDGMENTS

This study is supported by Nanyang Technological University (NTU) and Singapore Centre for 3D Printing (SC3DP), Singapore. Q.V. is supported by NTU Research Scholarship.

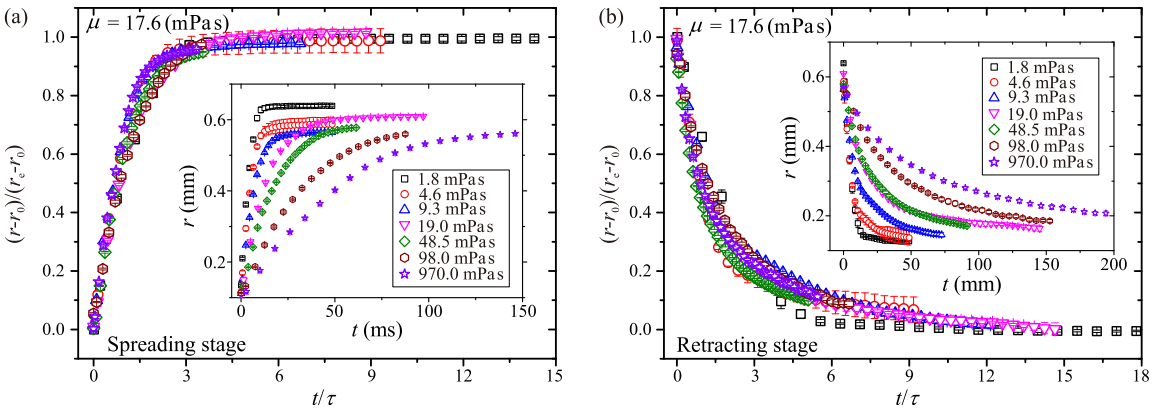

FIG. 6. Linear plots of the collapsed data of experiments with different oil's viscosity μ_o for spreading stage (a) and retracting stage (b). The raw data of each plot is shown by the corresponding inset.

[1] P. G. De Gennes, Rev. Mod. Phys. **57**, 827 (1985).
[2] D. Bonn, J. Eggers, J. Indekeu, J. Meunier, and E. Rolley, Rev. Mod. Phys. **81**, 739 (2009).
[3] R. V. Craster and O. K. Matar, Rev. Mod. Phys. **81**, 1131 (2009).
[4] F. Mugele and J.-C. Baret, J. Phys. Condens. Matter **17**, R705 (2005).
[5] P. Roach, N. J. Shirtcliffe, and M. I. Newton, Soft Matter **4**, 224 (2008).
[6] K. Choi, A. H. C. Ng, R. Fobel, and A. R. Wheeler, Annu. Rev. Anal. Chem. **5**, 413 (2012).
[7] Q. Vo, H. Su, and T. Tran, Sci. Rep. **8**, 836 (2018).
[8] J. C. Bird, S. Mandre, and H. A. Stone, Phys. Rev. Lett. **100**, 234501 (2008).
[9] J. Hong, Y. K. Kim, K. H. Kang, J. M. Oh, and I. S. Kang, Langmuir **29**, 9118 (2013).
[10] L. H. Tanner, J. Phys. D: Appl. Phys. **12**, 1473 (1979).
[11] T. D. Blake and J. M. Haynes, J. Colloid Interface Sci. **30**, 421 (1969).
[12] P. K. Mondal, D. DasGupta, A. Bandopadhyay, U. Ghosh, and S. Chakraborty, Phys. Fluids **27**, 032109 (2015).
[13] A. Eddi, K. G. Winkels, and J. H. Snoeijer, Phys. Fluids **25**, 013102 (2013).
[14] A. Carlson, G. Bellani, and G. Amberg, Europhys. Lett. **97**, 44004 (2012).
[15] D. Bartolo, C. Josserand, and D. Bonn, J. Fluid Mech. **545**, 329 (2005).
[16] J. Hong, Y. K. Kim, K. H. Kang, J. Kim, and S. J. Lee, Sens. Actuator B-Chem. **196**, 292 (2014).
[17] A. Carlson, M. Do-Quang, and G. Amberg, J. Fluid Mech. **682**, 213 (2011).
[18] A. Carlson, G. Bellani, and G. Amberg, Phys. Rev. E **85**, 045302(R) (2012).
[19] D. Duvivier, D. Seveno, R. Rioboo, T. D. Blake, and J. De Coninck, Langmuir **27**, 13015 (2011).
[20] C. A. Miller and L. E. Scriven, J. Fluid Mech. **32**, 417 (1968).
[21] C. Huh and L. E. Scriven, J. Colloid Interface Sci. **35**, 85 (1971).
[22] P. García-Sánchez, A. Ramos, and F. Mugele, Phys. Rev. E **81**, 015303(R) (2010).
[23] R. B. Fair, Microfluid Nanofluidics **3**, 245 (2007).
[24] J. Buehrle, S. Herminghaus, and F. Mugele, Phys. Rev. Lett. **91**, 086101 (2003).
[25] A. Staicu and F. Mugele, Phys. Rev. Lett. **97**, 167801 (2006).
[26] H. J. J. Verheijen and M. W. J. Prins, Langmuir **15**, 6616 (1999).
[27] C. Decamps and J. De Coninck, Langmuir **16**, 10150 (2000).
[28] J. C. Baret, M. M. J. Decré, and F. Mugele, Langmuir **23**, 5173 (2007).
[29] J. C. Baret, M. M. J. Decré, S. Herminghaus, and R. Seemann, Langmuir **23**, 5200 (2007).
[30] G. Lagubeau, M. A. Fontelos, C. Josserand, A. Maurel, V. Pagneux, and P. Petitjeans, J. Fluid Mech. **713**, 50 (2012).
[31] C. Redon, F. Brochard-Wyart, and F. Rondelez, Phys. Rev. Lett. **66**, 715 (1991).